Preservation of Image Content in Stain-to-stain Translation for Digital Pathology

Boqiang Huang[1], Wissem Benjeddou[2], Nadine S. Schaadt[3], Johannes Lotz[4], Friedrich Feuerhake[3,5], Dorit Merhof[1,6]

[1]Institute of Image Analysis and Computer Vision, University of Regensburg, Regensburg
[2]Institute of Imaging and Computer Vision, RWTH Aachen University, Aachen
[3]Institute for Pathology, Hannover Medical School, Hannover
[4]Fraunhofer Institute for Digital Medicine MEVIS, Lübeck
[5]Institute for Neuropathology, University Clinic Freiburg, Freiburg
[6]Fraunhofer Institute for Digital Medicine MEVIS, Bremen
Dorit.Merhof@ur.de

Abstract. In digital pathology, unsupervised domain adaptation of differently stained whole-slide images (WSIs) through image-to-image translation has become increasingly important for various applications such as stain augmentation or for the stain-independent application of deep learning models. In previous work, different variants of generative adversarial networks (GANs) were proposed to translate a real WSI obtained in the staining domain A into a fake WSI in the target staining domain B. However, GANs perform unpaired image-to-image translation and do not enforce consistency with respect to image content, which limits their applicability in digital pathology settings. In this paper, we first investigate the tissue inconsistency problem in such a stain-to-stain translation scenario using a quantitative evaluation of the distortion between real and fake images in different domains. Then, we investigate two possible solutions, namely (1) stain colorization inspired by natural image colorization, and (2) a modified Cycle-GAN, where an intensity invariant loss is proposed to balance the tissue consistency across staining domains. Our results highlight the superiority of these methods compared to conventional unpaired stain translation solutions for typical staining protocols in digital pathology.

1 Introduction

The extensive digitalization of histology glass slides using slide scanners, resulting in digital whole-slide images (WSIs), along with advancements in software and hardware, collectively referred to as digital pathology, has opened new opportunities for automated, highly precise, and reproducible quantification in pathology. To observe tissue samples comprehensively from multiple perspectives, it is common practice to stain consecutive tissue slides with different staining protocols, each sensitive to various tissue components (Fig. 1).

In recent research, neural network based approaches were developed to translate a given real WSI in staining domain A (e.g., PAS) into a fake WSI in the target staining domain B (e.g., H&E), or vice versa (Fig. 3) [1]. Typical applications of those stain translation approaches in digital pathology are stain augmentation [1, 2], image segmentation [3], and cancer classification [4].

C. Palm et al. (Hrsg.), *Bildverarbeitung für die Medizin 2025*, Informatik aktuell,
https://doi.org/10.1007/978-3-658-47422-5_26

Various approaches were so far investigated to realize unpaired stain translation of WSIs and other images, that mainly rely on the concept of generative adversarial networks (GANs). Initially, image colorization [5, 6] and image translation [7, 8] approaches were proposed. Later, Cho et al. [9] constructed a "de-stain" and "re-stain" network based on style transfer learning. Lin et al. [10] adapted this concept for unpaired multi-domain stain transfer, eliminating the necessity to train multiple models for different pairs of staining protocols. Similar to the Star-GAN and its modification [11], only one generator is trained for all possible many-to-many stain translations. Other GAN-based approaches address the stain variance problem by developing stain normalization methods to translate the raw WSIs into stain normalized images [12].

Actually, both image colorization [5, 6] and image translation [8] do have their own weaknesses in stain translation problems. For example, the former has to face non-unique colorization difficulties [2] while the latter can only guarantee the cycle consistency between staining domains [1, 2]. Despite extensive exploration of various network variants and losses, e.g., deformation invariant [13], structure- and/or edge-preserving [4, 14], segmentation consistency [3], multi-scale consistency [15], and contrastive learning-based similarity loss [16], there is no straightforward solution yet to the above-mentioned difficulties. Thus, these methods cannot guarantee that the translated image in the target domain retains the same tissue texture and structural information as the image in the original domain.

In this work, we propose a novel unsupervised stain-to-stain translation based on a pixel-level tissue consistency constraint. Section 2 presents the mathematical representation of both image colorization and image translation problems. Section 3 introduces our clinically meaningful intensity invariant loss compared to the conventional identity loss, together with two incisive distortion measures from both deterministic and statistical points of view. In section 4, experiments based on two independent kidney and breast WSI datasets highlight the outstanding performance of the proposed loss in unsupervised stain translation.

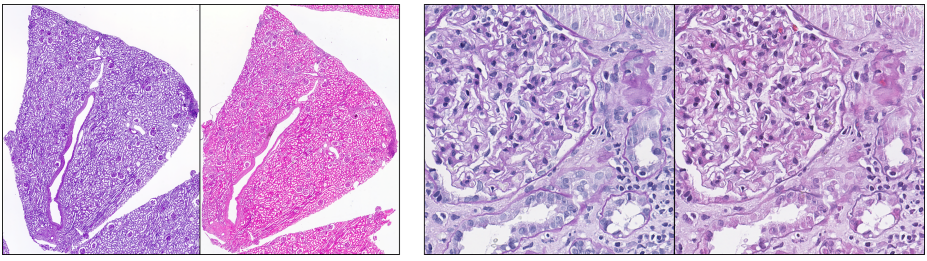

Fig. 1. Consecutive whole slide images of a kidney tissue sample stained in PAS and H&E (*left*), compared with a real image patch in PAS and its fake version in H&E (*right*) after applying the proposed stain translation method.

2 Background: stain colorization & stain translation

2.1 Color representations

A stained WSI, mathematically defined as a matrix $I \in \mathbb{R}^{H\times W\times 3}$, can be represented either in RGB space or CIE LAB space (Fig. 2). Let the nonlinear mapping relationship between these two spaces be $\mathcal{M}^{\text{RGB}\leftrightarrow\text{Lab}}$, both forward and inverse transforms will be

$$I^{\text{Lab}} = \mathcal{M}^{\text{RGB}\rightarrow\text{Lab}}\left[I^{\text{RGB}}\right] \tag{1}$$

$$I^{\text{RGB}} = \mathcal{M}^{\text{RGB}\leftarrow\text{Lab}}\left[I^{\text{Lab}}\right] \tag{2}$$

2.2 Supervised stain colorization

Given a staining protocol A, the colorization network C_{A} is trained for a nonlinear mapping relationship. The intensity $I_{\text{T}}^{\text{L}} \in \mathbb{R}^{H\times W}$ from the ground truth $I_{\text{T}} \in \mathbb{R}^{H\times W\times 3}$ is the input while the colorized fake image $I_{\text{F}}^{\text{RGB}} \in \mathbb{R}^{H\times W\times 3}$ is the output

$$I_{\text{F}}^{\text{RGB}} := C_{\text{A}}\left[I_{\text{T}}^{\text{L}}\right] \tag{3}$$

Since $\left(I^{\text{a}}, I^{\text{b}}\right)$ and I^{L} are paired, the training of a stain colorization network is supervised.

Moreover, the colorization can be further separated into two steps: the color estimation (from real intensity I_{T}^{L} to fake color pair $\left(I_{\text{F}}^{\text{a}}, I_{\text{F}}^{\text{b}}\right)$ and an inverse transform (from the fake CIE LAB $\left(I_{\text{T}}^{\text{L}}, I_{\text{F}}^{\text{a}}, I_{\text{F}}^{\text{b}}\right)$ to the fake RGB $I_{\text{F}}^{\text{RGB}}$)

$$\left(I_{\text{F}}^{\text{a}}, I_{\text{F}}^{\text{b}}\right) = C_{\text{A}}^{\text{Lab}}\left[I_{\text{T}}^{\text{L}}\right] \tag{4}$$

$$I_{\text{F}}^{\text{RGB}} := \mathcal{M}^{\text{RGB}\leftarrow\text{Lab}}\left[\left(I_{\text{T}}^{\text{L}} I_{\text{F}}^{\text{a}}, I_{\text{F}}^{\text{b}}\right)\right] \tag{5}$$

It should be noted that $C_{\text{A}}^{\text{Lab}} : I^{\text{L}} \rightarrow \left(I^{\text{a}}, I^{\text{b}}\right)$ cannot be a perfect one-to-one mapping relationship, since it is not possible to correctly estimate the color of a pixel only based on its optical intensity [5, 6]. Further, since C_{A} is trained with the knowledge in A, it would wrongly colorize a pixel from an unknown domain B with high probability, which would be uncontrollable and risky for any stain-to-stain translation.

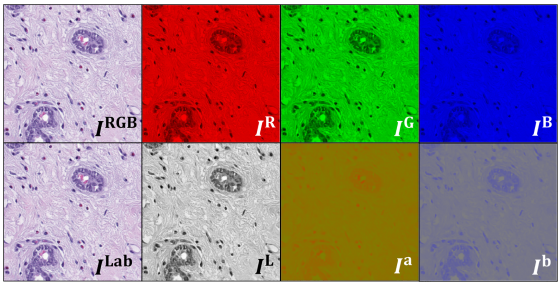

Fig. 2. WSI image $I \in \mathbb{R}^{H\times W\times 3}$ represented as I^{RGB} or I^{Lab} in RGB or a CIE LAB color space. Here, I^{R}, I^{G}, and I^{B} represent the red, green, and blue channels, while I^{L}, I^{a}, and I^{b} represent the optical intensity, green-to-red, and blue-to-yellow channels.

2.3 Unsupervised stain translation

Given two staining protocols A and B, the stain translation network $\mathcal{T}_{\mathrm{A}\leftrightarrow\mathrm{B}}$ is trained between unpaired WSI patches $I_{\mathrm{TA}}, I_{\mathrm{TB}} \in \mathbb{R}^{H\times W\times 3}$ in terms of unsupervised learning. The directional translations can be written as

$$I_{\mathrm{FB}} \coloneqq \mathcal{T}_{\mathrm{A}\to\mathrm{B}}\left[I_{\mathrm{TA}}\right] \tag{6}$$

$$I_{\mathrm{FA}} \coloneqq \mathcal{T}_{\mathrm{A}\leftarrow\mathrm{B}}\left[I_{\mathrm{TB}}\right] \tag{7}$$

where I_{FB} and I_{FA} denote the fake images of I_{TA} and I_{TB} in domain B and A, respectively. The so-called cycle-translation can then be written as

$$I_{\mathrm{RA}} \coloneqq \mathcal{T}_{\mathrm{A}\leftarrow\mathrm{B}}\left[I_{\mathrm{FB}}\right] = \mathcal{T}_{\mathrm{A}\leftarrow\mathrm{B}}\left[\mathcal{T}_{\mathrm{A}\to\mathrm{B}}\left[I_{\mathrm{TA}}\right]\right] \tag{8}$$

$$I_{\mathrm{RB}} \coloneqq \mathcal{T}_{\mathrm{A}\to\mathrm{B}}\left[I_{\mathrm{FA}}\right] = \mathcal{T}_{\mathrm{A}\to\mathrm{B}}\left[\mathcal{T}_{\mathrm{A}\leftarrow\mathrm{B}}\left[I_{\mathrm{TB}}\right]\right] \tag{9}$$

where I_{RA} and I_{RB} denote the reconstructed image of I_{TA} and I_{TB} in domain A and B, respectively. Since the reconstructed images should be the same as their corresponding inputs, the cycle-consistency loss is derived as follows (Fig. 3, top)

$$\mathcal{L}_{\mathrm{cyc}}\left(\mathcal{T}_{\mathrm{A}\leftrightarrow\mathrm{B}}\right) \coloneqq \mathbb{E}_{I\sim p_{\mathrm{data}}}\left\{\left\|I_{\mathrm{TA}} - I_{\mathrm{RA}}\right\|_1\right\} + \mathbb{E}_{I\sim p_{\mathrm{data}}}\left\{\left\|I_{\mathrm{TB}} - I_{\mathrm{RB}}\right\|_1\right\} \tag{10}$$

Here, the ℓ_1 norm is applied as in Cycle-GANs [1, 3, 8].

Now, by combining the standard adversarial loss functions in domain A and B

$$\mathcal{L}_{\mathrm{advA}} \coloneqq \mathbb{E}_{I\sim p_{\mathrm{data}}}\left\{\log\left(1 - \mathcal{D}_{\mathrm{A}}\left(I_{\mathrm{FA}}\right)\right)\right\} + \mathbb{E}_{I\sim p_{\mathrm{data}}}\left\{\log\left(\mathcal{D}_{\mathrm{A}}\left(I_{\mathrm{TA}}\right)\right)\right\} \tag{11}$$

$$\mathcal{L}_{\mathrm{advB}} \coloneqq \mathbb{E}_{I\sim p_{\mathrm{data}}}\left\{\log\left(1 - \mathcal{D}_{\mathrm{B}}\left(I_{\mathrm{FB}}\right)\right)\right\} + \mathbb{E}_{I\sim p_{\mathrm{data}}}\left\{\log\left(\mathcal{D}_{\mathrm{B}}\left(I_{\mathrm{TB}}\right)\right)\right\} \tag{12}$$

with the cycle-consistency loss in Eq. (10), the optimization problem of a Cycle-GAN is

$$\mathcal{T}^{*}_{\mathrm{A}\leftrightarrow\mathrm{B}} = \arg\min_{\mathcal{T}_{\mathrm{A}\leftrightarrow\mathrm{B}}} \max_{\mathcal{D}_{\mathrm{A}},\mathcal{D}_{\mathrm{B}}} \mathcal{L}\left(\mathcal{T}_{\mathrm{A}\leftrightarrow\mathrm{B}}, \mathcal{D}_{\mathrm{A}}, \mathcal{D}_{\mathrm{B}}\right) \tag{13}$$

$$\mathcal{L}\left(\mathcal{T}_{\mathrm{A}\leftrightarrow\mathrm{B}}, \mathcal{D}_{\mathrm{A}}, \mathcal{D}_{\mathrm{B}}\right) = \mathcal{L}_{\mathrm{advA}} + \mathcal{L}_{\mathrm{advB}} + \lambda_{\mathrm{cyc}} \cdot \mathcal{L}_{\mathrm{cyc}}\left(\mathcal{T}_{\mathrm{A}\leftrightarrow\mathrm{B}}\right) \tag{14}$$

where $\mathcal{D}_{\mathrm{A}}$ and $\mathcal{D}_{\mathrm{B}}$ represent the discriminator in domain A and B, respectively.

3 Method: intensity invariant stain translation

3.1 Distortion measures

In order to quantitatively evaluate structural distortions between real and fake images, the peak signal-to-noise ratio (PSNR) and the similarity index measure (SSIM) are considered. Let I_{t} and I_{f} represent the target image and reference image with the same dimension, the PSNR is defined as

$$d_{\mathrm{PSNR}}\left(I_{\mathrm{t}}, I_{\mathrm{f}}\right) \coloneqq 10\log_{10}\left(\frac{1}{\frac{1}{\#I}\left\|I_{\mathrm{t}} - I_{\mathrm{f}}\right\|_2^2}\right) \tag{15}$$

where $\#I$ denotes the cardinality of the image.

Different from the Euclidean metric, the SSIM is designed based on a perception model that considers image degradation as perceived change in structural information

$$d_{\text{SSIM}}\left(I_{\text{t}}, I_{\text{f}}\right) \coloneqq \frac{\left(2\mu_{\text{t}}\mu_{\text{f}} + c_1\right)\left(2\sigma_{\text{tf}} + c_2\right)}{\left(\mu_{\text{t}}^2 + \mu_{\text{f}}^2 + c_1\right)\left(\sigma_{\text{t}}^2 + \sigma_{\text{f}}^2 + c_2\right)} \tag{16}$$

where μ and σ represent the pixel sample mean and standard deviation, c_1 and c_2 represent two controllable constants that can stabilize the division with weak denominator.

3.2 Identity loss

Recall that the cycle-consistency is actually a very loose constraint for image translation problems. Thus, the authors in [1, 3, 8] found that it is helpful to introduce an additional loss to Eq. (14) such that the mappings $\mathcal{T}_{\text{A}\leftrightarrow\text{B}}$ are encouraged to preserve the color composition between the input and output

$$\mathcal{L}_{\text{idt}}\left(\mathcal{T}_{\text{A}\leftrightarrow\text{B}}\right) \coloneqq \mathbb{E}_{I\sim p_{\text{data}}}\left\{\|I_{\text{TA}} - \mathcal{T}_{\text{A}\leftarrow\text{B}}\left[I_{\text{TA}}\right]\|_1\right\} + \mathbb{E}_{I\sim p_{\text{data}}}\left\{\|I_{\text{TB}} - \mathcal{T}_{\text{A}\rightarrow\text{B}}\left[I_{\text{TB}}\right]\|_1\right\} \tag{17}$$

Since the input image is taken from the target domain, the presented loss is more similar to an identity loss (Fig. 3 Bottom Left). This loss is considered in comparison to our novel intensity invariant loss proposed in Section 3.3.

3.3 Intensity invariant loss

Assuming that the tissue sample is not damaged in the staining, it is reasonable to require the invariant intensity of both the input real WSI patch in the source domain and the output fake WSI patch in the target domain (Fig. 3 Bottom Right). Accordingly, we propose a novel loss function as follows

$$\mathcal{L}_{\text{int}}\left(\mathcal{T}_{\text{A}\leftrightarrow\text{B}}\right) \coloneqq \mathbb{E}_{I\sim p_{\text{data}}}\left\{\|I^{\text{L}}_{\text{TA}} - I^{\text{L}}_{\text{FB}}\|_1\right\} + \mathbb{E}_{I\sim p_{\text{data}}}\left\{\|I^{\text{L}}_{\text{TB}} - I^{\text{L}}_{\text{FA}}\|_1\right\} \tag{18}$$

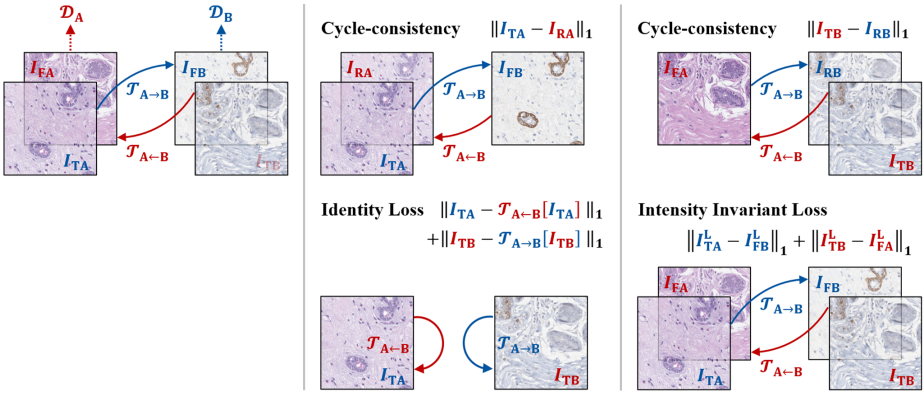

Fig. 3. Stain translation is achieved using a naive Cycle-GAN with cycle-consistency constraints (top), identity loss (bottom left), and intensity-invariant loss (bottom right).

4 Experiments and results

4.1 Datasets

Dataset D1 consists of human kidney samples stained in PAS and H&E protocols. There are five renal transplant samples stained in H&E. Another eight renal specimens were stained in PAS. The WSI image patch was tiled with 512×512 pixels. There were 3000 patches randomly selected for training (1500 PAS + 1500 H&E), and 500 patches randomly selected from the rest for testing (250 PAS + 250 H&E).

Dataset D2 consists of both healthy and cancerous breast samples which are stained in CK5/14 and H&E protocols. There are eight samples stained in H&E and fifteen samples stained in CK5/14. Each WSI image patch is tiled at 512×512 pixels, and then down-sampled to 256×256 pixels to reduce the computational load. There are 16000 images randomly selected for training (8000 CK5/14 + 8000 H&E), and 4000 images randomly selected for testing (2000 CK5/14 + 2000 H&E).

All WSI images were scanned with a 40X objective lens (ca. 0.25 microns per pixel (mpp)) using Aperio scanners from Leica[1].

4.2 Stain colorization results

Four stain colorization networks have been trained based on both datasets D1 and D2, which are marked by C_{PAS}, $C_{\text{HE-1}}$, C_{CK}, and $C_{\text{HE-2}}$. Here, HE-1 and HE-2 are two different

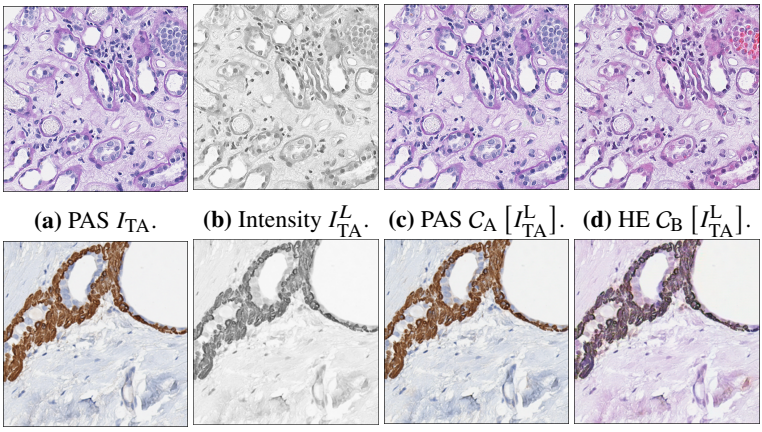

(a) PAS I_{TA}. **(b)** Intensity I^{L}_{TA}. **(c)** PAS $C_{\text{A}}\left[I^{\text{L}}_{\text{TA}}\right]$. **(d)** HE $C_{\text{B}}\left[I^{\text{L}}_{\text{TA}}\right]$.

(e) CK I_{TA}. **(f)** Intensity I^{L}_{TA}. **(g)** CK $C_{\text{A}}\left[I^{\text{L}}_{\text{TA}}\right]$. **(h)** HE $C_{\text{B}}\left[I^{\text{L}}_{\text{TA}}\right]$.

Fig. 4. Stain colorization and colorization-based stain translation. (a) and (e) are real images in PAS and CK5/14 domains, respectively. (b) and (f) are intensity images. (c) and (g) are colorized fake images. (d) and (h) are colorization-based translation results in the target H&E domain (no ground truth for comparison).

[1] www.leicabiosystems.com

datasets from D1 and D2, respectively. Network settings are the same as the ones in [8]. Visual results are shown in Fig. 4.

Tab. 1 illustrates that the colorization networks can learn the nonlinear relationship between the intensity and the color very well. Moreover, when the provided dataset is large enough, such as in D2, the immunohistochemical staining method can be learned with high accuracy.

4.3 Stain translation results

Based on the Cycle-GAN loss in Eq. (14), the identity loss in Eq. (17), and the intensity invariant loss in Eq. (18), three experiments were designed to investigate the contribution of these constrains in stain translation.

- *Scenario 1*: Cycle-GAN with neither identity loss nor intensity invariance loss
  Since the cycle-consistency loss Eq. (10) is the only constraint for the translation, the generator can certain a good reconstruction but cannot maintain a qualified translation in the target domain [8]. As shown in Fig. 5b and 5f, many unreasonable tissue components are generated in the target domain, which results in inconsistent tissue details between the original domain and the target domain. Such phenomenon can be observed in Tab. 2 as well, in which d^1_{PSNR} is the smallest one and d^1_{SSIM} values are all negative.
- *Scenario 2*: Cycle-GAN with identity loss but without intensity invariant loss
  In this case, the total loss function is updated as

$$\mathcal{L}\left(\mathcal{T}_{\mathrm{A}\leftrightarrow\mathrm{B}}, \mathcal{D}_{\mathrm{A}}, \mathcal{D}_{\mathrm{B}}\right) = \mathcal{L}_{\mathrm{advA}} + \mathcal{L}_{\mathrm{advB}} + \lambda_{\mathrm{cyc}} \cdot \mathcal{L}_{\mathrm{cyc}} + \lambda_{\mathrm{idt}} \cdot \mathcal{L}_{\mathrm{idt}} \tag{19}$$

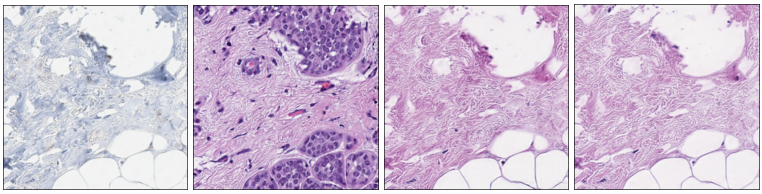

(a) CK I_{TA}. **(b)** HE, $\mathcal{T}^1_{\mathrm{A}\to\mathrm{B}}[I_{\mathrm{TA}}]$. **(c)** HE, $\mathcal{T}^2_{\mathrm{A}\to\mathrm{B}}[I_{\mathrm{TA}}]$. **(d)** HE, $\mathcal{T}^3_{\mathrm{A}\to\mathrm{B}}[I_{\mathrm{TA}}]$.

(e) HE I_{TB}. **(f)** CK, $\mathcal{T}^1_{\mathrm{A}\leftarrow\mathrm{B}}[I_{\mathrm{TB}}]$. **(g)** CK, $\mathcal{T}^2_{\mathrm{A}\leftarrow\mathrm{B}}[I_{\mathrm{TB}}]$. **(h)** CK, $\mathcal{T}^3_{\mathrm{A}\leftarrow\mathrm{B}}[I_{\mathrm{TB}}]$.

Fig. 5. Stain translation in different cases. (a) and (e) are real images in CK5/14 and H&E domains respectively. (b) and (f) are translated images in Case-1. (c) and (g) are translated images in Case-2. (d) and (h) are translated images in Case-3.

Tab. 1. Stain colorization performance.

$d_{(\cdot)}(I_T, I_F)$	C_{PAS}		$C_{HE\text{-}1}$		C_{CK}		$C_{HE\text{-}2}$	
$I_F \coloneqq C_{(\cdot)}[I_T]$	Train	Test	Train	Test	Train	Test	Train	Test
d_{PSNR}	33.31	33.17	30.99	30.83	38.43	38.24	36.23	36.08
d_{SSIM}	0.97	0.97	0.96	0.96	0.97	0.97	0.98	0.98

Tab. 2. Stain translation performance.

$d_{(\cdot)}(I_T^L, I_F^L)$	$\mathcal{T}_{PAS\to HE}$		$\mathcal{T}_{PAS\leftarrow HE}$		$\mathcal{T}_{CK\to HE}$		$\mathcal{T}_{CK\leftarrow HE}$	
$I_F \coloneqq \mathcal{T}_{(\cdot)}[I_T]$	Train	Test	Train	Test	Train	Test	Train	Test
d^1_{PSNR}	10.58	10.53	11.33	11.30	12.58	12.54	13.06	13.22
d^1_{SSIM}	−0.30	−0.30	−0.33	−0.34	−0.30	−0.30	−0.30	−0.29
d^2_{PSNR}	19.45	19.53	17.29	17.37	18.25	18.22	18.09	18.20
d^2_{SSIM}	0.80	0.80	0.77	0.78	0.81	0.81	0.82	0.82
d^3_{PSNR}	22.80	22.38	21.85	21.50	24.79	26.38	23.63	24.05
d^3_{SSIM}	0.89	0.88	0.89	0.89	0.91	0.92	0.87	0.88

Similar to the setting in [1, 3, 8], the weighting coefficients λ_{cyc} and λ_{idt} are set to 1 (i.e., equal contribution of all loss terms).
Tab. 2 shows that the identity loss can preserve the content and therefore constraint the behavior of the generator. Comparing to the Case-1, all distortion measures had been improved significantly.

- *Scenario 3*: Cycle-GAN with both identity loss and intensity invariant loss
  Now, all the proposed loss terms are integrated into

$$\mathcal{L}(\mathcal{T}_{A\leftrightarrow B}, \mathcal{D}_A, \mathcal{D}_B) = \mathcal{L}_{advA} + \mathcal{L}_{advB} + \lambda_{cyc} \cdot \mathcal{L}_{cyc} + \lambda_{idt} \cdot \mathcal{L}_{idt} + \lambda_{int} \cdot \mathcal{L}_{int} \quad (20)$$

  In practice, the weighting coefficients λ_{cyc}, λ_{idt}, and λ_{int} are set to 1 as well.

Fig. 5 shows that there is no substantial structural difference in the intensity image among the real image, the translated image in Case-2, and the translated image in Case-3. Tab. 2 quantitatively shows that Case-3 achieves the smallest distortion or the largest similarity d^3_{PSNR} and d^3_{SSIM} among all three cases. However, Fig. 5g and 5h still exhibits the color nonuniqueness problem, which cannot be quantitatively compared as there is no ground truth in the target domain.

5 Conclusion

In this study, we reviewed the color representation in histopathological stain translation, including stain colorization and stain translation. We highlight the advantages and disadvantages of both stain colorization and stain translation in practical applications. In detail, colorization worked more accurately if the staining domain is unchanged. Otherwise, the multi-domain stain translation should be considered in order to alleviate the color non-uniqueness problem, where more constraints are introduced into unsupervised

deep learning solutions, e.g., by introducing identity loss and the proposed intensity invariant loss into the Cycle-GAN. Since we seriously consider the tissue texture distortion at the pixel level in terms of PSNR and SSIM, we avoid higher distortions between the images from the source and the target staining domains, as observed for methods based on geometry- / topology- / morphology- / statistics-induced loss functions.

Acknowledgement. This study was supported by the BMBF (Project No. FKZ 01IS21067A-C, FKZ 01ZX1608A), and the DFG (Project No. 445703531). The authors gratefully acknowledge the computational and data resources provided by the Leibniz Supercomputing Centre (`www.lrz.de`).

References

1. Gadermayr M, Gupta L, Appel V et al. Generative adversarial networks for facilitating stain-independent supervised and unsupervised segmentation: a study on kidney histology. IEEE Trans Med Imaging. 2019;38(10):2293–302.
2. Haan K de, Zhang Y, Zuckerman JE et al. Deep learning-based transformation of H&E stained tissues into special stains. Nat Commun. 2021;12(4884).
3. Bouteldja N, Klinkhammer BM, Schlaich T et al. Improving unsupervised stain-to-stain translation using self-supervision and meta-learning. J Pathol Inform. 2022;13(100107).
4. Berijanian M, Schaadt NS, Huang B et al. Unsupervised many-to-many stain translation for histological image augmentation to improve classification accuracy. J Pathol Inform. 2023;14(100195).
5. Nazeri K, Ng E, Ebrahimi M. Image colorization using generative adversarial networks. Proc AMDO. 2018:85–94.
6. Vitoria P, Raad L, Ballester C. ChromaGAN: adversarial picture colorization with semantic class distribution. Proc IEEE CVF WACV. 2020:2445–54.
7. Choi Y, Choi M, Kim M et al. StarGAN: unified generative adversarial networks for multi-domain image-to-image translation. Proc IEEE CVF CVPR. 2018:8789–97.
8. Zhu JY, Park T, Isola P et al. Unpaired image-to-image translation using cycle-consistent adversarial networks. Proc IEEE ICCV. 2017:2223–32.
9. Cho H, Lim S, Choi G et al. Neural stain-style transfer learning using GAN for histopathological images. Proc ACML. 2017.
10. Lin Y, Zeng B, Wang Y et al. Unpaired multi-domain stain transfer for kidney histopathological images. Proc AAAI. 2022:1630–7.
11. Choi Y, Uh Y, Yoo J et al. StarGAN v2: diverse image synthesis for multiple domains. Proc IEEE CVF CVPR. 2020:8188–97.
12. Bentaieb A, Hamarneh G. Adversarial stain transfer for histopathology image analysis. IEEE Trans Med Imaging. 2018;37(3):792–802.
13. Wang C, Yang G, Papanastasiou G et al. DiCyc: GAN-based deformation invariant cross-domain information fusion for medical image synthesis. Inf Fusion. 2021;67:147–60.
14. Wagner SJ, Khalili N, Sharma R et al. Structure-preserving multi-domain stain color augmentation using style-transfer with disentangled representations. Proc MICCAI. 2021:257–66.
15. Liu S, Zhu C, Xu F et al. BCI: breast cancer immunohistochemical image generation through pyramid Pix2pix. Proc IEEE CVF CVPR. 2022:1815–24.

16. Li F, Hu Z, Chen W et al. Adaptive supervised PatchNCE loss for learning H&E-to-IHC stain translation with inconsistent groundtruth image pairs. Proc MICCAI. 2023:632–41.